Biological Procedures Online

RESEARCH

Open Access

Uncovering Novel Susceptible Genes and Therapeutic Targets of Prostate Cancer: a Multi-omics Study Integrating Summary-based Mendelian Randomization Analysis and Molecular Docking

Xuemeng Qiu[1,2†], Yifei Zhang[1,2†], Jiyue Wu[1,2†], Zihao Gao[1,2], Xinyi Chai[3], Xihao Shen[1,2], Zejia Sun[1,2*†] and Wei Wang[1,2*]

Abstract

Background Understanding the role of causal genes of prostate cancer (PrCa) can reveal key biological pathways and identify potential targets for treatment.

Methods We investigated associations between genetically predicted gene expression levels and PrCa risk using cis-eQTL summary-based Mendelian randomization (SMR) and colocalization analysis. Findings were replicated using two independent PrCa GWAS. We then intersected the identified genes with differentially expressed genes (DEGs) identified from TCGA-PRAD dataset to obtain key genes. Furthermore, enrichment, protein-molecule network, immune infiltration, and epigenetic analyses were conducted to explore their biological pathways. Lastly, phenome-wide association study (PheWAS), drug prediction, and molecular docking simulation analysis were utilized to identify potential drugs.

Results We identified 15 genes in blood whose expression levels are putatively associated with PrCa, validated in at least one replication GWAS dataset. Using open-access mRNA-sequencing data, we found that *ZNF217* and *BNIP2* were key genes potentially important in PrCa pathogenesis. Single-cell RNA-sequencing analysis revealed that *BNIP2* was predominantly expressed in a subset of endothelial cells, whereas *ZNF217* was mainly enriched in epithelial cells. Downstream analysis revealed their involvement in epigenetic modulation-related pathways, while upstream analysis showed that upregulation of *ZNF217* notably correlated with increased CpG methylation. Molecular docking simulation suggested doxorubicin, alsterpaullone, and camptothecin as potential drugs targeting these key genes.

†Xuemeng Qiu, Yifei Zhang, Jiyue Wu and Zejia Sun contributed equally to this work.

*Correspondence:
Zejia Sun
mnwkszj5076@163.com
Wei Wang
weiwang0920@163.com

Full list of author information is available at the end of the article

Conclusions These findings provide robust leads for understanding pathogenic mechanisms and developing therapeutic interventions for PrCa.

Keywords Mendelian randomization, Prostate cancer, Molecular docking, Drug discovery, Epigenetic

Introduction

Prostate cancer (PrCa) accounts for approximately 7% of all newly diagnosed cancers in men worldwide, translating to over 1.2 million new cases and 375,000 deaths annually [1, 2]. Despite significant advancements in management strategies—ranging from active surveillance and prostatectomy to definitive radiation, androgen deprivation therapy, and emerging focal therapies—the treatment of advanced PrCa remains challenging [3]. The underlying genetic pathogenesis of PrCa is not yet fully understood, largely due to the disease's heterogeneous nature [4]. Therefore, there is still a pressing need for molecular biomarkers to investigate potential therapeutic targets to improve treatment outcomes for PrCa.

Mendelian randomization (MR) analysis, which uses genetic variants as instrumental variables, is increasingly used to investigate causal relationships between traits [5]. Expression quantitative trait loci (eQTLs) identify genetic variants that influence gene expression levels. Integration of summary-level data from GWAS and eQTL using SMR analysis [6] predicts genes whose expression levels are associated with complex traits because of pleiotropy (one genetic variant affects both gene expression and the interested trait). Furthermore, heterogeneity-independent instrument (HEIDI) tests have been employed to distinguish potential causal associations amidst extensive linkage disequilibrium (LD) across the genome [7], mitigating confounding and reverse causation. The SMR-HEIDI method can reach a much higher statistical power than conventional two-sample MR techniques when exposure and outcome are available from two independent samples with robust sample sizes [6].

Extensive bioinformatic investigation into the pathogenesis of PrCa has been conducted in recent years, leveraging data from transcriptomics, epigenetics, transcriptional profiling, metabolomics, and more [8]. In terms of genomic data, although GWAS studies can identify genetic variants associated with a certain trait, the genetically predicted causal variants are often located in non-coding regions of the genome, making it difficult to connect them to specific functional genes. Previous MR studies mainly focused on genetically predicted plasma proteins and the risk of PrCa [9, 10]. However, a limited level of colocalization between causal eQTLs and pQTLs was observed, indicating distinct differences in mRNA versus protein in their origin and biological property [11]. A few MR studies investigated associations between specific phenotypic (mitochondrial-related, senescence-related) gene expression and multiple cancer types, including PrCa, but without detailed downstream or upstream explorations [12, 13]. Therefore, there is a lack of focused studies exploring causal associations of gene expression and PrCa. Thus, integrating SMR analysis with traditional bioinformatics approaches, such as epigenetic analysis, is invaluable for identifying novel potential therapeutic targets in PrCa.

This study presents an SMR-based multi-omics approach to identify potential causal effects of gene expression on PrCa using blood and prostate tissues. We first integrated PrCa GWAS summary statistics from three distinct sources with eQTLs in the blood using SMR-HEIDI analysis and verified causal genetic variants using colocalization analysis. We then extracted differentially expressed genes (DEGs) identified by a large mRNA-sequencing dataset and intersected them with SMR-identified key genes. Additional analyses on prognostic significance, genetic alteration landscape, immune cell infiltration, and pathway enrichment were conducted to explore the upstream and downstream effects of these key genes. Finally, we performed drug prediction and molecular docking simulations to explore the potential therapeutic significance of the significant genes.

Materials and Methods

Data Sources

Exposure data: Summary-level data of SNP-gene expression associations were found on the eQTLGen consortium website (https://www.eqtlgen.org/cis-eqtls.html). Specifically, SMR-formatted cis-eQTL results (.epi,.esi,.besd) were downloaded, which contain 19,250 genes in at least 2 cohorts that showed expression in blood and were on autosomal chromosomes. Tissue-specific cis-eQTL results from the V8 release of the Genotype-Tissue Expression (GTEx) consortium were directly downloaded from the Yang Lab website (https://yanglab.westlake.edu.cn/software/smr/#DataResource). This set of data contains cis-eQTL summary data across 49 human tissues from the GTEx project. The current study focused on cis (local)-eQTLs, which are SNPs located near regulatory regions of genes and are known to exert more direct and pronounced effects on gene expression compared to trans (distant)-eQTLs. Accordingly, SNPs located within 1 Mb of the transcription start site were selected, as this window encompasses most functional cis-regulatory elements through local chromatin interactions [14]. To ensure statistical rigor, only associations with gene expression reaching a significance threshold of $P < 1e\text{-}5$ was included, consistent with the criteria

Table 1 Detailed information of the GWAS datasets used

Dataset	Sample sizes (*N* control vs. *N* cases)	Ancestry	Consortium	Reference
PrCa GWAS	140,254 (61,106 vs. 79,148)	European	PRACTICAL	https://www.ebi.ac.uk/gwas/studies/GCST006085
	182,625 (9132 vs. 173493)	European	UK Biobank	https://gwas.mrcieu.ac.uk/
	146,465 (131266 vs. 15199)	European	FinnGen R10 release	https://www.finngen.fi/en/access_results

Abbreviations: *PrCa* prostate cancer, *N control* number of controls, *N cases* number of cases, *PRACTICAL* Prostate Cancer Association Group to Investigate Cancer Associated Alterations in the Genome, *GWAS* genome-wide association study

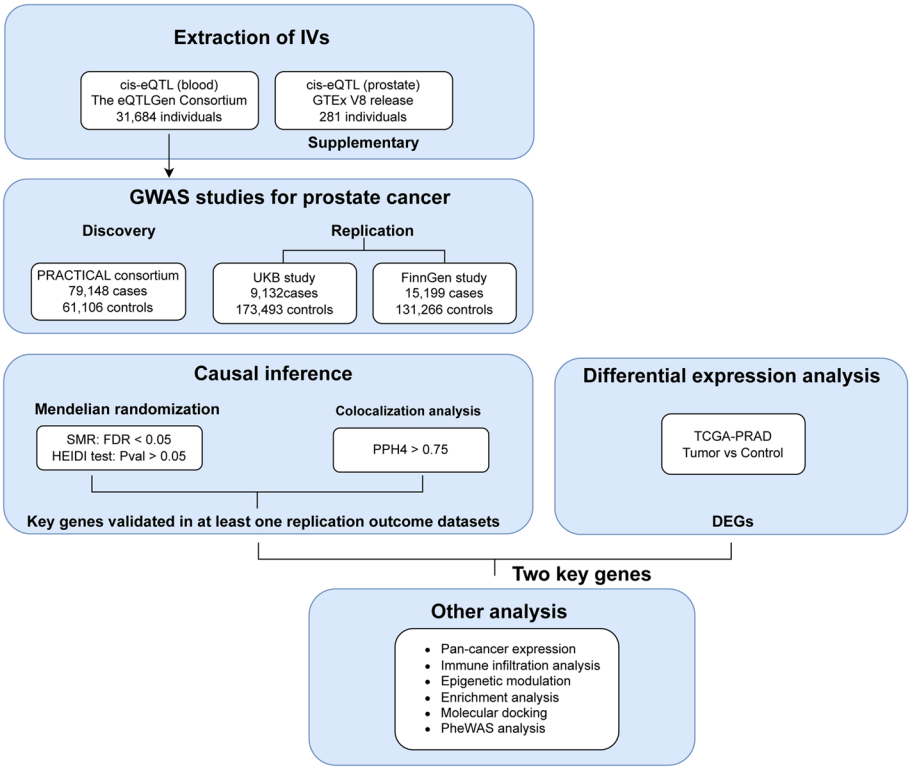

Fig. 1 Study workflow

described in the reference database (https://yanglab.westlake.edu.cn/software/smr/#DataResource).

Outcome data: GWAS studies of prostate cancer from 3 distinct sources were included. Summary statistics of GWAS results from the PRACTICAL consortium were used as the discovery cohort [15], while GWAS results from the UK biobank (UKB) and FinnGen were used as validation cohorts. All individuals involved are of European ancestry. A detailed description of the GWAS datasets used is provided in Table 1.

For mRNA sequencing data of prostate adenocarcinoma, we used standardized TCGA-PRAD cancer samples and TCGA-PRAD cohort control samples, integrated with normal prostate tissue from the GTEx project. These data were obtained from the TARGET Pan-Cancer (PANCAN) project via the UCSC Xena browser (https://xenabrowser.net/). The database contai ns RNA sequencing expression data from 9,736 tumors and 8,587 normal tissues, sourced from the TCGA and GTEx projects using a standard processing protocol. The study design was shown in Fig. 1.

Processed single-cell RNA sequencing (scRNA-seq) data of prostate cancer dataset (PRAD-GSE141445) [16] was downloaded from the TISCH database (http://tisch.compbio.cn/home/), which included 12 primary and 1 lymph node metastasis tissue samples from 12 patients. For validation scRNA-seq dataset, processed scRNA-seq data of prostate adenocarcinoma biopsies were obtained [17], which contained a set of 15,492 cells, grouped by tumor and normal tissue. Uniform Manifold Approximation and Projection (UMAP) was used for dimensional reduction and visualization for both datasets.

SMR Analysis

SMR analysis is specifically designed for testing pleiotropic association between the expression level of a gene and

a trait (eQTL-GWAS association). This approach adheres to the three fundamental assumptions of MR: (1) robust SNP-exposure associations; (2) absence of confounding relationships between SNPs and outcomes; (3) SNPs are only associated with the outcome through the exposure. The SMR software (Mac version) was used for SMR analysis using the default parameters provided by the official website. The SMR analysis also includes the HEIDI test that excludes causality caused by linkage disequilibrium. Therefore, SNPs inclusion criteria from SMR and HEIDI test are as follows: (1) False discovery rate (FDR) adjusted p value from SMR < 0.05; (2) p value from HEIDI test > 0.05; (3) a minor allele frequency (MAF) > 0.01. The included SNPs are used as instrumental variables (IVs). The study adheres to STROBE-MR guidelines (Supplementary Table 1).

Colocalization Analysis

Bayesian colocalization analysis was performed to assess whether the exposure and outcome phenotypes have shared common genetic causal variants in a given region. Analyses were performed using the "coloc" R package (https://github.com/chr1swallace/coloc, version 5.2.3) using default parameters. Posterior probabilities for colocalization are: (1) H0: neither trait have a genetic association; (2) H1/H2: only trait 1/2 has a genetic association in the region; (3) H3: both traits are associated, but with different causal variants; (4) H4: both traits are associated with a shared single causal variant. A posterior possibility ≥ 75% provides strong evidence that genetic variants regulate these genes and influence the observed outcome through gene expression.

Phenome-wide Association Studies

To avoid horizontal pleiotropy, we used the IEU OpenGWAS project (https://gwas.mrcieu.ac.uk/phewas/) website to obtain the potential associated traits of SNPs corresponding to the identified genes.

Differential mRNA Expression, Enrichment, and Immune Cell Infiltration Analysis

Differentially expressed genes (DEGs) analysis of the TCGA dataset was performed by setting |log2FC| threshold as 0.5 and using the "limma" method. For pan-cancer assessment of the identified genes (BNIP2 and ZNF217), we extracted the expression data of these two genes across samples from the following sources: solid tissue normal, primary solid tumor, primary tumor, normal tissue, primary blood- derived cancer (bone marrow and peripheral blood). For normalization, we applied log2(x + 0.001) transformation to each expression value. Finally, we excluded cancer types with fewer than 3 samples, ultimately obtaining expression data for 34 cancer types. Additionally, we performed survival analysis based on the median expression of the two-gene signature and generated the Kaplan-Meier curve (K-M curve) using the GEPIA online website. Similar gene detection was also used to identify putative co-expressed genes, therefore inferring potential upstream-downstream pathways using Pearson correlation analysis. Co-expressed genes are defined as Pearson correlation coefficient (PCC) > 0.5.

To explore functional biological pathways of identified genes, Gene Ontology (GO) and Kyoto Encyclopedia of Genes and Genomes (KEGG) enrichment analysis were performed using the "clusterProfiler" R package (version 4.4.4).

To assess the association with immune cell infiltration, we used the "ESTIMATE" R package [18] to calculate each sample's stromal and immune scores. We evaluated the correlation between genes and stromal/immune scores using Pearson's correlation coefficient. We also calculated cell infiltration proportion using the TIMER [19], quanTIseq [20], MCPCounter [21] and EPIC [22] algorithms. We conducted all these analyses on the Sangerbox website (http://vip.sangerbox.com/home.html), a platform specifically designed for TCGA-GTEx data analysis.

Genetic Alteration and Epigenetic Modulation Landscape

To investigate transcriptional alterations and epigenetic modulations of the two genes, we first examined gene alteration types in all non-overlapping prostate carcinoma studies and stratified them by detailed cancer type on the cBioportal database (https://www.cbioportal.org/). This database contains information about mutations, putative DNA copy number data using the GISTIC algorithm, and other clinical data with corresponding large consortium studies, like TCGA and TARGET. The results were visualized by cBioportal and the Sangerbox website.

Furthermore, we utilized the SMART website (http://www.bioinfo-zs.com/smartapp/), which utilizes methylation data of the TCGA project, to explore methylation levels of ZNF217 and BNIP2 in the tumor and normal group. Initially, we compared the median degrees of CpG methylation of the two genes in tumor and normal groups. Then, we obtained gene-related CpG probes and explored their expression levels in the tumor and normal groups. Lastly, the correlation between gene expression and DNA methylation was analyzed.

Protein-Chemical Interaction Analysis

Protein-chemical interaction networks can enhance drug development. STITCH (http://stitch.embl.de/) [23] is an online platform that integrates and visualizes extensive chemical and protein interactions, including tissue-specific ones. We input all significant genes inferred from SMR analysis to explore their interactions, then assessed the two key genes and their interactions with chemicals

within prostate tissue by selecting "use RNA-seq data" from the Human Protein Atlas.

Drug Prediction and Molecular Docking Simulation Analysis

Enrichr and the Drug Signatures Database (DSigDB) were used to predict potential drug molecules. Enrichr (https://maayanlab.cloud/Enrichr/) contains about 400,000 annotated gene sets [24], including a vast repository of drug and small molecule-related gene sets [25]. DSigDB was accessed through Enrichr's Diseases/Drugs function, then potential therapeutic drugs and molecules were ranked based on their combined scores. We selected the top three candidates: doxorubicin (DOX), alsterpaullone, and camptothecin (CPT). The selection was based on the fact that these three drugs have already been used in cancer treatment but are not routinely used in PrCa. This makes them ideal candidates for molecular docking analyses to identify new therapeutic targets.

Molecular docking simulation was used to investigate interactions between potential drugs and the two target genes—a method widely used in drug discovery to predict ligand-target interactions at the molecular level. The crystal protein structures were obtained from the RCSB Protein Data Bank (https://www.rcsb.org/) and the AlphaFold Protein Structure Database (https://alphafold.ebi.ac.uk/). We downloaded "3D-SDF" format structure files of potential drugs from the PubChem database (https://pubchem.ncbi.nlm.nih.gov/). Using PyMOL 2.5.8 and AutoDockTools 1.5.7, we modified protein structures by removing existing ligands and water molecules, adding hydrogen atoms, optimizing amino acids, and calculating charges. In this context, drugs served as ligands while protein structures of the genes acted as receptors. We used AutoDock Vina to predict binding conformations between ligands and receptors. To assess potential binding affinity, we used binding energy, a weighted average of the docking score. Values above −4 kcal/mol indicate weak interactions, −4 to −7 kcal/mol suggest moderate binding, and below −7 kcal/mol indicate strong binding affinity. Finally, we visualized molecular interactions using PyMOL 2.5.8.

Statistical Analysis

Statistical analyses were performed using R software (version 4.2.1). For comparisons between two groups, Wilcoxon rank-sum and signed-rank tests were used, while the Kruskal-Wallis test was employed for comparisons among more than two groups. The Chi-square test was used to evaluate the differences in gene mutation frequency in each group of samples. Pearson correlation analysis was used to determine the correlation between variables. Statistical significance was defined as $p < 0.05$.

Results

Candidate Risk Genes of Prostate Cancer Identified by SMR Analysis

We first conducted SMR analysis to examine associations between blood gene eQTLs and prostate cancer GWAS from 3 sources. Manhattan plots showing the chromosomal distribution of these significant genes are displayed in Fig. 2. The Main PRACTICAL dataset revealed 180 blood genes significantly associated with prostate cancer (PrCa) (FDR < 0.05, p HEIDI > 0.05), while the FinnGen and UK Biobank (UKB) datasets yielded 24 and 51 significant associations, respectively (Supplementary Table 2). To ensure the credibility of the results, we intersected the significant genes of the PRACTICAL dataset (discovery) with either the UKB or FinnGen dataset (replication), identifying 15 genes that were confirmed in a validation dataset. Results for causal effects of blood gene eQTLs and PrCa are presented in Fig. 3a, with SIK2 gene expression being validated in all three datasets. After filtering for colocalization evidence (PPH4 > 0.75, replicated in the validation dataset), genetically predicted higher expression levels of *BNIP2* (OR: 1.208, 95% CI: 1.116–1.299, PPH4 = 0.808), *SLC39A1* (OR: 1.267, 95% CI: 1.200–1.334, PPH4 = 0.950), and *ZNF217* (OR: 1.123, 95% CI: 1.054–1.192, PPH4 = 0.793) are positively associated with PrCa risk. Genetically predicted higher expression levels of *TBPL1* (OR: 0.841, 95% CI: 0.759–0.923, PPH4 = 0.923) and *TRIM8* (OR: 0.784, 95% CI: 0.715–0.852, PPH4 = 0.852) are associated with lower risk of PrCa in the discovery dataset. Additionally, associations for prostate-tissue specific gene eQTLs and PrCa were also analyzed (Supplementary Table 2). Given the significant role of immune regulation in both the development and progression of PrCa, we chose to focus primarily on blood eQTLs.

Then we explored the mechanisms of the identified genes. GO and KEGG enrichment analysis indicated these genes are involved in viral oncogenesis pathway, T cell receptor binding, and epigenetic modulation, such as RNA polymerase II core promoter sequence-specific DNA binding (Fig. 3b). Protein-protein interactions using the STITCH database revealed 3 main clusters: ZNF217 and TBPL1 interacted with each other through CTBP1 and HDAC2 molecules; BNIP2 interacted with CDC42 and SPAG9 protein molecules; and SIK2 interacted with CRTC2 (Fig. 3c).

Differential Expression Analysis and SMR Identified *ZNF217* and *BNIP2* as Putative Key Genes in PrCa

To prioritize genes that not only show expression differences in disease but also have genetic evidence supporting their causal roles in PrCa rather than being a downstream effect, we intersected DEGs from the

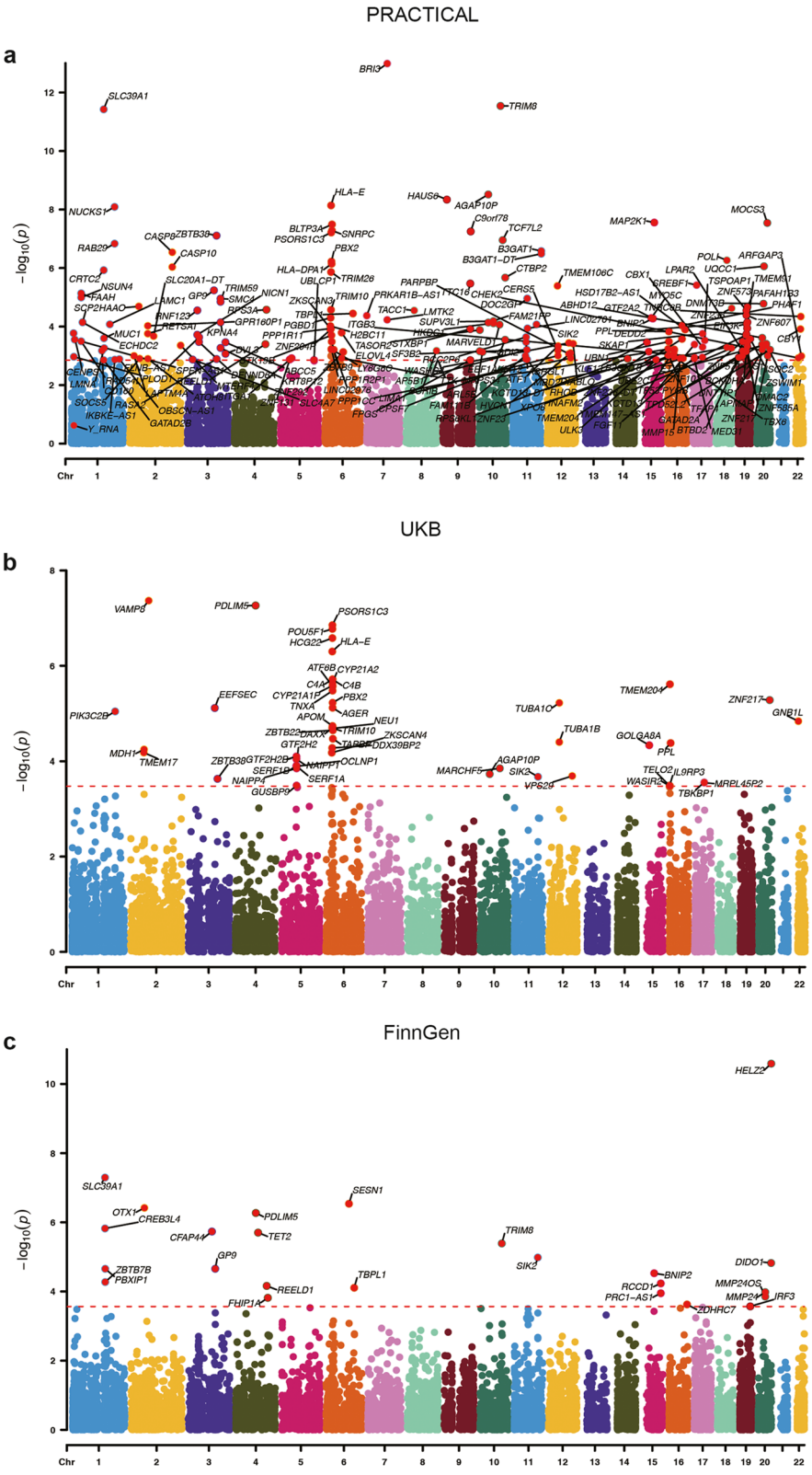

Fig. 2 Manhattan plot for associations between blood gene expression and prostate cancer. Manhattan plot for blood gene expression and outcome data from (**a**) PRACTICAL, **b** UKB, **c** FinnGen consortiums. Abbreviation: PRACTICAL, Prostate Cancer Association Group to Investigate Cancer Associated Alterations in the Genome; UKB, UK Biobank; Chr, chromosome

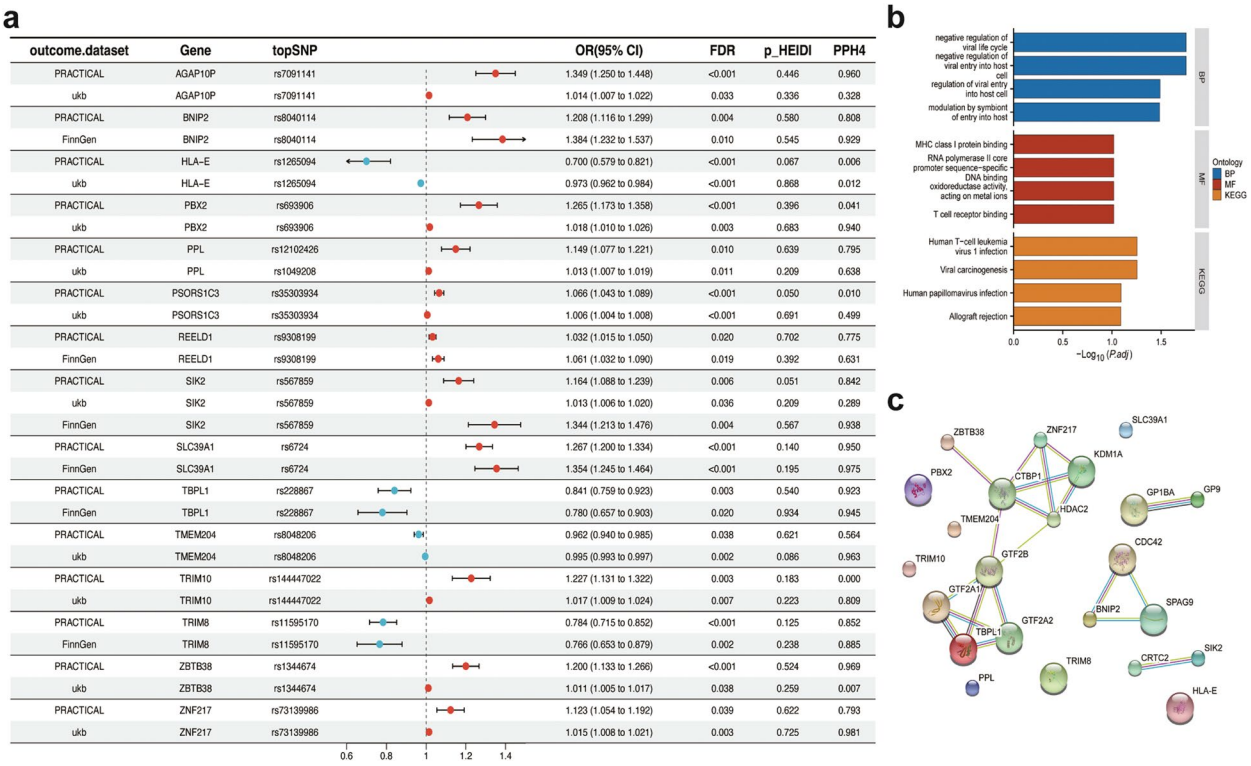

Fig. 3 Key genes identified by SMR analysis and their downstream effects. **a** Forest plot of the significant genes (FDR < 0.05, p_HEIDI > 0.05, PPH4 > 0.75) identified by SMR, replicated in the validation dataset. **b** GO and KEGG enrichment analysis of the significant genes. **c** Protein-protein interaction network of the significant genes. Abbreviation: SNP, single-nucleotide polymorphism; OR, odds ratio; FDR, false discovery rate; p_HEIDI, p value of heterogeneity-independent instrument test; PPH4, posterior probability of hypothesis 4; BP, biological process; MF, molecular function; KEGG, Kyoto Encyclopedia of Genes and Genomes; GO, Gene Ontology

TCGA-PRAD dataset with SMR- identified causal genes, resulting in *ZNF217* and *BNIP2* (Fig. 4a). Patients with higher scores of the two-gene signature exhibited worse overall survival (Fig. 4b), indicating a strong correlation with disease prognosis. To gain a comprehensive understanding of these two genes across various cancer types, we analyzed their differential expression between tumor tissue and adjacent normal tissue. As shown in Fig. 4c-d, *ZNF217* generally displayed significantly higher expression in tumor tissue across most cancer types, including PrCa ($p < 0.0001$). In contrast, *BNIP2* showed varied expression patterns across cancer types, with down-regulated expression observed in PrCa ($p < 0.001$).

Immune cell infiltration analysis revealed a significant inverse correlation between higher expression of *ZNF217* and immune score, while *BNIP2* demonstrated the opposite effect (Fig. 4e-f). Furthermore, *BNIP2* expression showed a positive correlation with the stromal score, whereas *ZNF217* had no significant association (Fig. 4g-h), suggesting that *ZNF217* predominantly influences immune infiltration, whereas *BNIP2* influences both immune and stromal cells (Fig. 4e-h). To further characterize the stromal effects of *BNIP2*, we utilized cell types deconvolution algorithms and examined moderate correlation of *BNIP2* expression with endothelial cells, cancer-associated fibroblasts (CAFs), and weak association with fibroblasts (Supplementary Fig. 1). Despite the inverse association between *ZNF217* expression and overall immune infiltration, our analysis using the TIMER algorithm indicated a strong positive correlation with innate immune cells, such as neutrophils, macrophages, and dendritic cells (DCs). *BNIP2* expression was positively correlated with both innate and adaptive immune cells, including CD8 + T cells and B cells (Fig. 4i). These findings were further validated using the quanTIseq algorithm (Supplementary Fig. 2).

We next examined *BNIP2* and *ZNF217* expression at the single-cell level. A total of 19 cell clusters corresponding to eight cell types were identified and visualized in UMAP plots (Fig. 5a-b). Malignant, immune, and stromal lineages were distinguishable within the tumor microenvironment (Fig. 5c). The pie chart demonstrated epithelial cells being the most abundant population (Fig. 5d). To interrogate intercellular networks, we performed cell- cell communication analysis, which identified a specific endothelial subcluster (Endothelial_17)

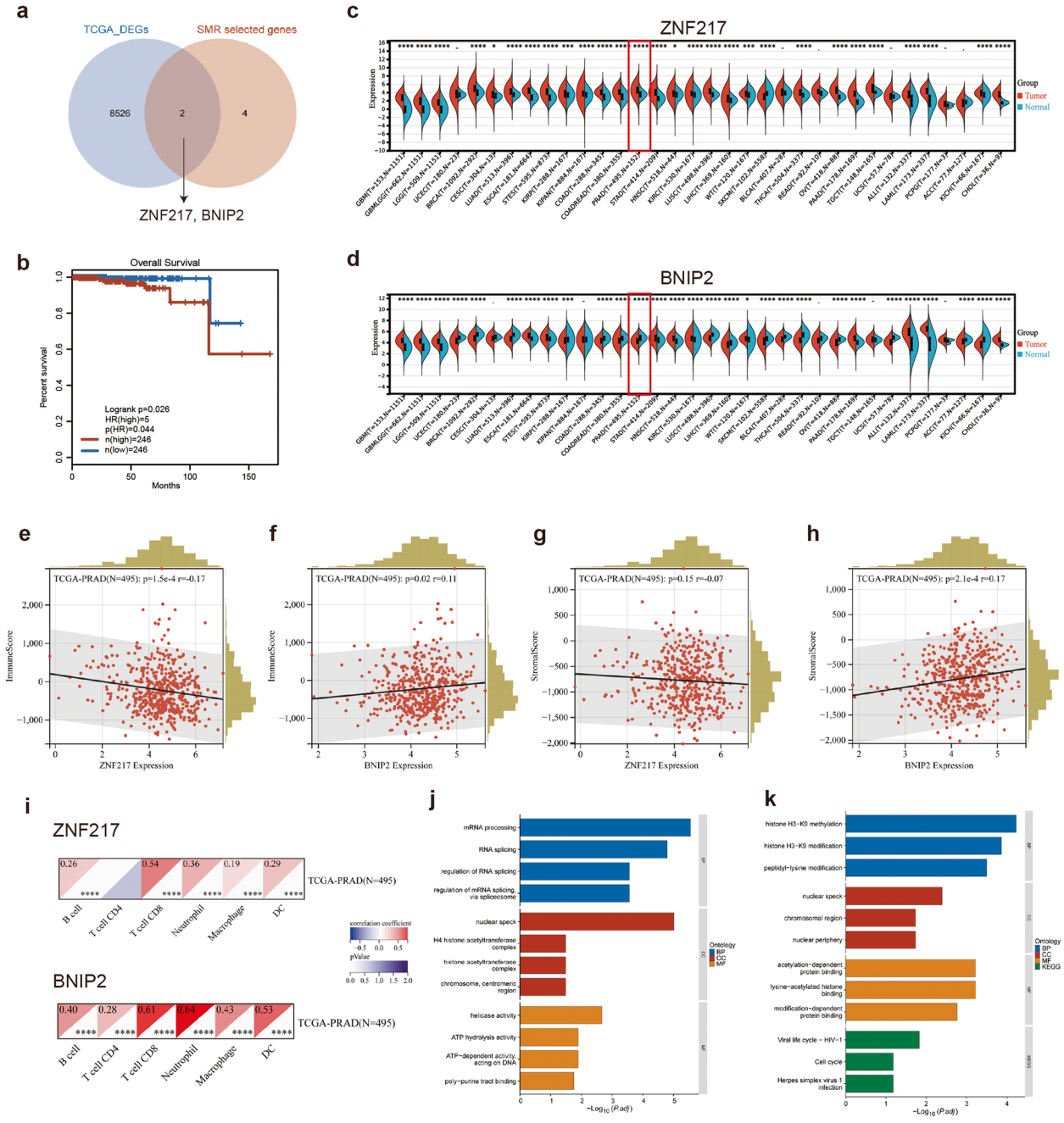

Fig. 4 The expression of *ZNF217* and *BNIP2* and their associations with clinical prognosis, immune characteristics and enriched pathways. **a** Venn plot of DEGs and SMR identified significant genes. **b** K-M survival plot of the 2 gene signature in prostate cancer patients. **c**-**d** The mRNA expression of *ZNF217* and *BNIP2* across cancer types. **e**-**h** The key genes expression and associations with immune and stromal scores. **i** Immune infiltration scores by TIMER algorithm. **j** GO and KEGG enrichment analysis of co-expressed genes for *ZNF217* and *BNIP2*, respectively. Abbreviation: TCGA, The Cancer Genome Atlas; DEGs, differentially expressed genes; K-M, Kaplan-Meier; DC, dendritic cells; BP, biological process; MF, molecular function; CC, cellular component KEGG, Kyoto Encyclopedia of Genes and Genomes; GO, Gene Ontology. *, $p < 0.05$; **, $p < 0.01$; ***, $p < 0.001$, ****, $p < 0.0001$

exhibiting robust autocrine signaling as well as active crosstalk with multiple epithelial subsets (Fig. 5e). Coincidentally, we observed *BNIP2* being highly expressed in this subset of endothelial cells, while *ZNF217* mostly expressed in malignant cells and epithelial cells in the microenvironment (Fig. 5f). Gene ontology enrichment of Endothelial_17 highlighted upregulated key processes including angiogenesis, regulation of cell migration, and response to transforming growth factorβ (Fig. 5g). These findings are also replicated in an independent scRNA-seq cohort of Tuong et al., where *BNIP2* remained highly expressed in endothelial cells, whereas *ZNF217*

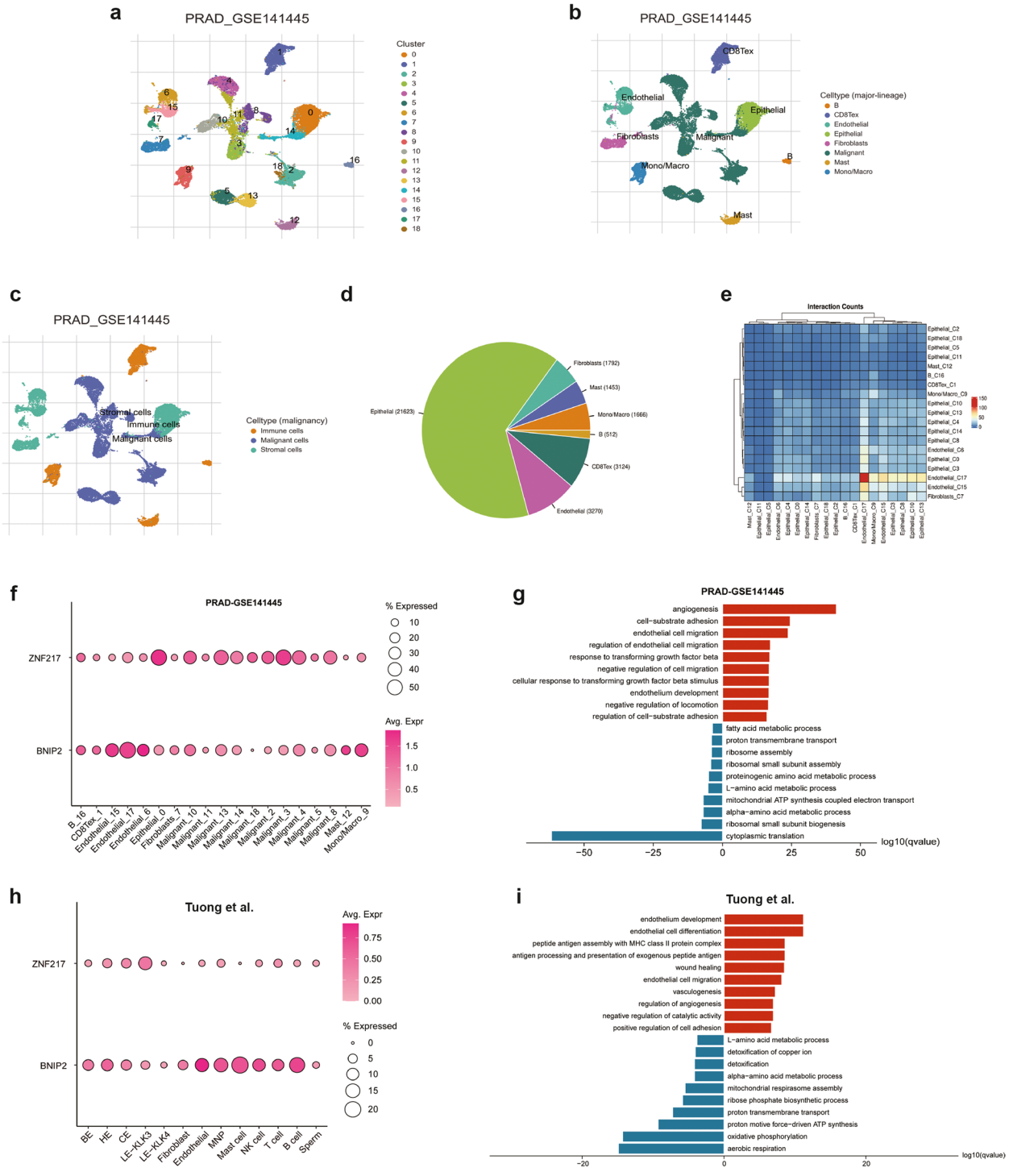

Fig. 5 *BNIP2* and *ZNF217* expression in single-cell RNA-sequencing data. **a**-**c** UMAP plots of cell clusters, cell types, and malignancy, respectively. **d** Cell proportion in the tumor microenvironment by pie chart. **e** Global cell-cell communication activity by heatmap. **f**, **h** Dot plot displaying gene expressions in each cell type. **g** GO enrichment of Endothelial_17 cell cluster. **i** GO enrichment analysis of tumor endothelial cells. Abbreviation: UMAP, Uniform Manifold Approximation and Projection; GO, Gene Ontology

specifically expressed in the luminal epithelial KLK3-positive subset-characterized by elevated androgen receptor levels and enrichment in multiple immune pathways (Fig. 5h-i).

To elucidate the downstream effects of *ZNF217* and *BNIP2*, we obtained the top 100 similar genes corresponding to the 2 genes in the PRAD tumor datasets on GEPIA website. The gene Lists are shown in

Supplementary Table 3, with all PCC well above 0.7. Enrichment analysis revealed that histone H3-K9 methylation and modification pathways are enriched in *ZNF217* and its co-expressed genes; while RNA splicing, mRNA processing, ATP activity pathways are enriched in *BNIP2* and its associated genes (Fig. 4j-k).

Epigenetic Modifications and Genetic Alterations of *ZNF217* and *BNIP2*

To investigate the epigenetic modifications and transcriptional alterations of *ZNF217* and *BNIP2*, we initially utilized cBioportal database. *ZNF217* was modified in 1.2% of the patients, with amplification being the predominant alteration type. *BNIP2* was modified in 0.6% of the patients, primarily through deep deletion (Fig. 6a). These alteration types were most frequent in prostate adenocarcinoma (Fig. 6b). For *BNIP2*, mutations occurred primarily in exon 3, with E126V encoding the most common mutated protein. For *ZNF217*, mutations clustered downstream of the Zinc-finger double domain (486–508), with H517D being the predominant mutated protein (Fig. 6c). The somatic landscape showed distinct gene alterations in high and low *ZNF217* expression groups with *TP53* and *SPOP* being the dominant altered genes. *TP53* ($p = 0.01$), *SPOP* ($p = 0.02$), *NALCN* ($p = 0.04$), *HFM1* ($p = 0.04$), and *TIAM* ($p = 0.04$) had significantly different mutated status between groups. Concurrently, low and high expression levels of *BNIP2* also showed distinct somatic landscape, with *FOXA1* ($p = 0.05$), *KDM6A* ($p = 0.02$), *TMPRSS2* ($p = 0.04$), and *HCN1*($p = 0.04$) displaying statistically different mutation frequency between groups (Fig. 6d). Furthermore, we analyzed *BNIP2* expression in PRAD samples using data from the TCGA pan-cancer cohort, assessing its association with copy number variation (CNV). The results showed that *BNIP2* expression was significantly lower in the Loss group compared to Neutral group (Fig. 6e), suggesting a potential link between *BNIP2* downregulation and CNV loss in PrCa. Collectively, we hypothesized that the decreased expression of *BNIP2* was attributable to deep deletion or CNV loss, while the altered expression of *ZNF217* in the tumor group was likely due to amplification.

We then examined the methylation levels of *ZNF217*, as expression levels and methylation levels are often inversely related. The mean CpG-aggregated methylation levels of *ZNF217* showed significantly decreased methylation ($p < 0.0001$) in tumor samples compared to normal samples in PrCa (Fig. 6f). Furthermore, when comparing the mean methylation of *ZNF217*-related CpG probes between normal and tumor groups in PrCa, ten probes (cg05359207, cg07617814, cg12032027, cg01692482, cg17098965, cg09029902, cg20979153, cg09228833, cg11551296, and cg15871544) showed hypomethylation in tumor tissue (Fig. 6g). The methylation levels of these probes generally displayed an inverse linear relationship with *ZNF217* expression (Fig. 6h), suggesting the hypomethylation of *ZNF217* might lead to its over-expression. Lastly, protein-protein interactions connected *BNIP2* and *ZNF217* through the HDAC protein family and BCL2 (Fig. 6i). In prostate tissue, protein-chemical network analysis revealed that BNIP2 interacts with MgATP, MgADP, and guanosine triphosphate, though ZNF217 did not exhibit significant interactions with small molecules in prostate tissue (Fig. 6j).

PheWAS Analysis

To rule out possible pleiotropy of IVs used, we conducted PheWAS analysis. rs73139986 (*ZNF217* expression related) was associated with secondary traits, such as gonococcal infection, insomnia, and keloid etc., while rs8040114 (*BNIP2* expression related) was associated with traits such as benign neoplasms of the uterus, shortsightedness, and disease of middle ear and mastoid etc. (Supplementary Table 4). These observations indicate potential side effects of targeting *ZNF217* and *BNIP2*, necessitating further investigations.

Drug Prediction and Molecular Docking Simulations for *ZNF217* and *BNIP2*

Using Enrichr and transcriptome signatures from the DSigDB, we predicted 68 potential therapeutic drugs, ranked by their combined scores (Supplementary Table 5). After a thorough evaluation, we identified DOX, alsterpaullone, and CPT as the top three candidates for further investigation in PCa treatment. The molecular docking results for six potential drugs and significant genes are presented in both macro and micro views (Fig. 7a-f). DOX demonstrated strong binding energies of −6.7 and − 7.3 kcal/mol with ZNF217 and BNIP2, respectively (Fig. 7a-b). Notably, its interactions with ZNF217 involved polar contacts with amino acids ALA-509, GLN-510, and TYR-485, while interactions with BNIP2 included LEU-223 and ARG-217. Alsterpaullone exhibited binding energies of −7.1 kcal/mol with both ZNF217 and BNIP2, forming polar contacts with ARG-481 in ZNF217 and with ARG-217 and LEU-223 in BNIP2 (Fig. 7c-d). CPT yielded binding energies of −6.6 and − 7.1 kcal/mol with ZNF217 and BNIP2, respectively, establishing polar contacts with HIS-489 in ZNF217 and ARG-217 and LEU-223 in BNIP2 (Fig. 7e-f). All metrics and deposits of the molecular docking are deposited in Additional file 1.

Discussion

In this study, we performed SMR and colocalization analyses to explore the potential causal relationship of genetically-predicted gene expression with prostate cancer. Then, combined with results from RNA sequencing

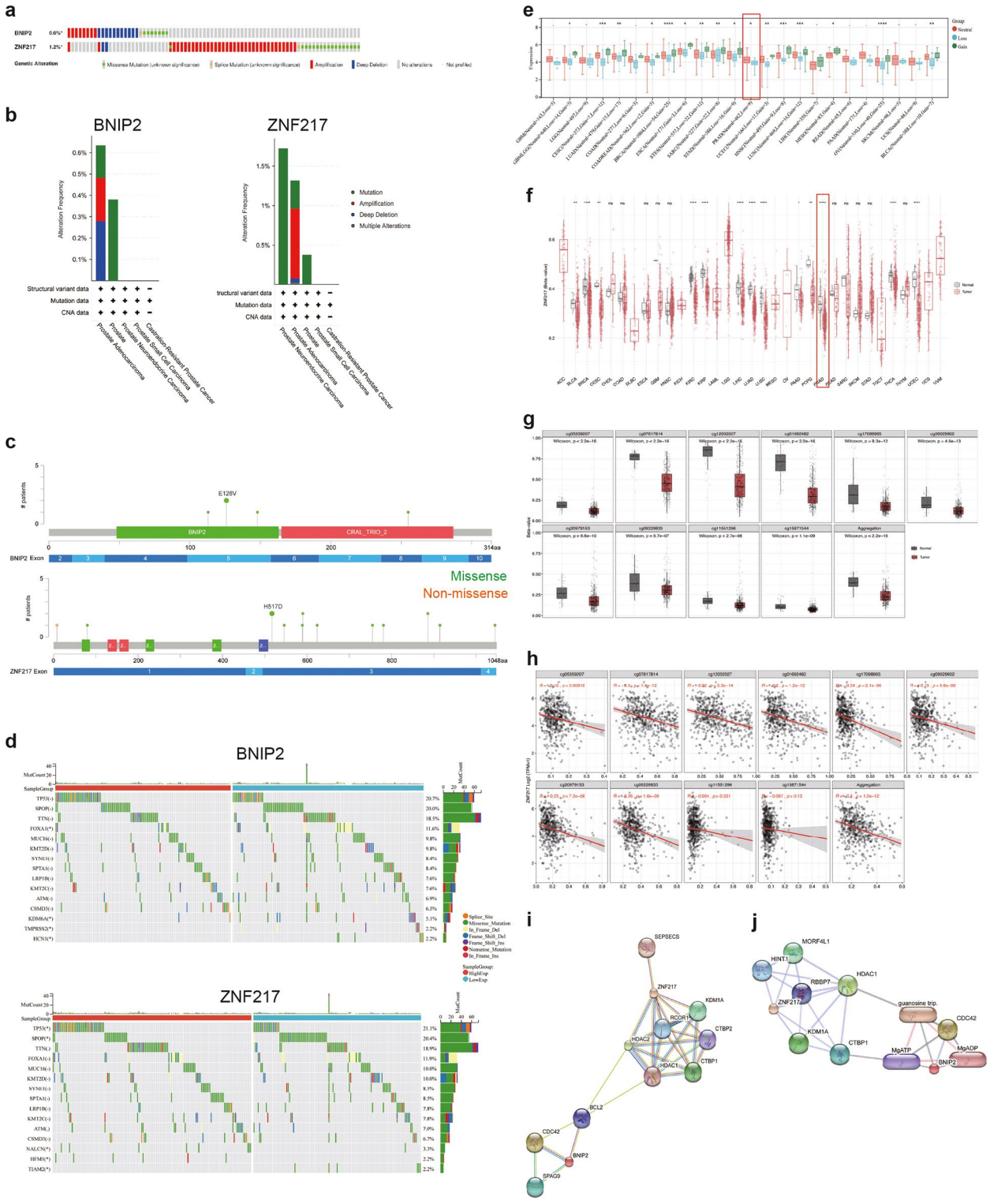

Fig. 6 Genetic alterations landscape of *ZNF217* and *BNIP2*. **a**-**b** Schematic diagrams illustrating the proportion and types of genetic alterations of the key genes across prostate cancer and its subtypes. **c** Mutation panels for *BNIP2* and *ZNF217* showing mutation frequency and location. The vertical axis represents the number of patients harboring each mutation, while the horizontal axis indicates the specific mutation sites within each gene. **d** Onco-plots showing the somatic landscape. **e** Box plots showing the CNV of *BNIP2* across cancer types. **f**-**g** CpG-aggregated methylation levels of *ZNF217* across cancer types and associated CpG probes. **h** Correlation between *ZNF217* expression and probe methylation levels. **i**-**j** Protein-protein, protein-molecule network of ZNF217 and BNIP2. Abbreviation: CNV, copy number variations. *, $p < 0.05$; **, $p < 0.01$; ***, $p < 0.001$, ****, $p < 0.0001$

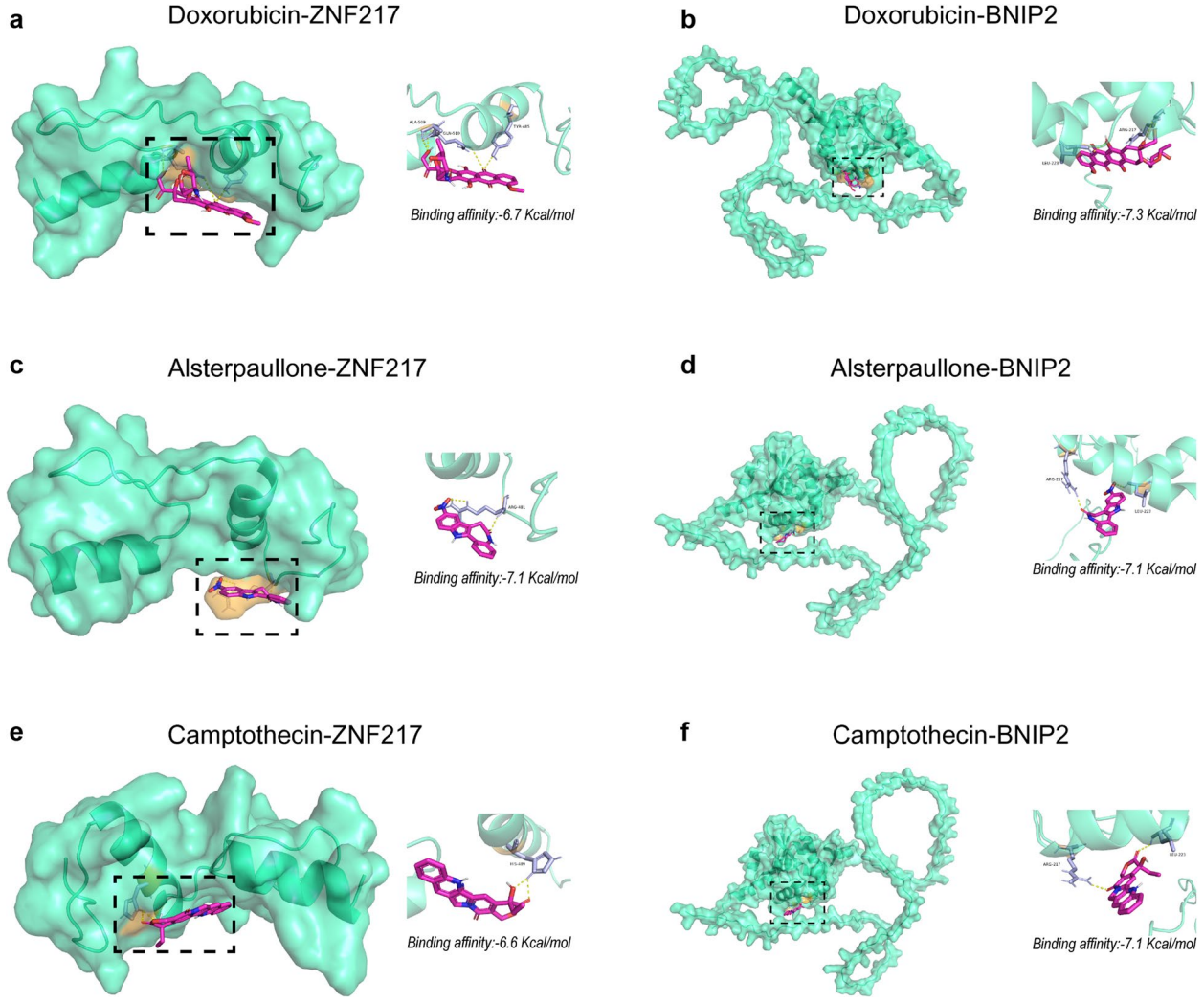

Fig. 7 Three-dimensional structure diagrams showing receptors and ligands by molecular docking. **a**-**c** Doxorubicin, alsterpaullone, and camptothecin with ZNF217, respectively. **d**-**f** Doxorubicin, alsterpaullone, and camptothecin with BNIP2, respectively

data and methylation data, we found that *ZNF217* and *BNIP2* gene expression were putatively associated with PrCa. High expression of *ZNF217* in PrCa was partially due to hypomethylation, while low expression of *BNIP2* was likely because of deep deletion. *ZNF217* and *BNIP2* mRNA expression and their correlation with prognosis, protein and molecular landscape, altered signal pathways, and immune infiltration were also investigated. Additionally, molecular docking simulation targeting the two genes was also performed. Our study linked genetic variants, gene expression, and DNA methylation to identify causal genes for PrCa.

Our study initially identified 15 genes putatively associated with PrCa using SMR analysis. We applied stringent criteria and required replication in at least one additional outcome dataset. Subsequent colocalization analysis suggested that genetic variants of five genes (*BNIP2*, *SLC39A1*, *ZNF217*, *TBPL1*, *TRIM8*) may act in a coordinated manner to either promote or protect against tumorigenesis. The specific variants identified were rs8040114, rs6724, rs73139986, rs228867, and rs11595170, respectively. A previous study demonstrated that m6A modification of *TRIM8* mRNA, which encodes the E3 ubiquitin ligase for the oncogenic gene *NFIB*, could decrease its translation and expression, thereby promoting *NFIB* stability [26]. Bioinformatic analyses have revealed *SLC39A1* overexpression in hepatocellular carcinoma and gliomas' cancerous tissue compared to adjacent normal tissue, although this has not been reported in prostate cancer. Knockdown of *SLC39A1* leads to upregulation of tumor-progression related proteins [27, 28]. While experimental studies on *TBPL1* in prostate cancer are lacking, a previous study utilizing SMR analysis investigating senescence-related genes across multiple cancer types found that *ZNF217* was associated with prostate cancer, while *TBPL1* expression

was negatively associated with PrCa [12]. Our study corroborated these findings, identifying *TBPL1* as a potential protective gene for PrCa, despite it not being identified as a DEG in the TCGA dataset. This discrepancy warrants further investigation into the relationship between SMR-identified risk or protective genes and DEGs that potentially contribute significantly to the disease process.

After intersecting SMR-identified genes with DEGs, *ZNF217* and *BNIP2* stood out as key genes that might regulate the progression of PrCa. *ZNF217*, a member of the Kruppel-like family of transcription factors, primarily binds to target gene promoters, functioning as a repressor that promotes cell proliferation and inhibits cell death. Its upregulation is associated with advanced stages of breast, pancreatic, ovarian, and colon cancers [29], establishing it as an oncogenic gene. However, its role in prostate cancer remains limited. Interactions with non-coding RNA networks and deregulated DNA methylation of *ZNF217* lead to aberrant expression of the oncogene itself. Additionally, the ZNF217 protein or complex orchestrates other genes' expression by modulating DNA methylation, H3K4 methylation, and H3K27 acetylation [30–32]. Our enrichment analysis of *ZNF217* and its co-expressed genes verified their potential downstream role in epigenetic modulation of other genes. However, reports of *ZNF217* in PrCa are scarce. Recent studies identified *ZNF217* as a target for microRNAs such as miR-24 and miR-503 in advanced PrCa, evidenced by in silico or in vitro research methods [33, 34], thus modulating the downstream epithelial–mesenchymal transition (EMT) pathway. Nevertheless, there is a lack of direct verification of *ZNF217*'s causal roles in PrCa. Previous studies have found that *ZNF217* amplification is among the most frequent genetic alterations, and its overexpression is associated with unfavorable outcomes in breast cancer or ovarian clear cell carcinoma, as shown by quantitative real-time PCR DNA copy gain analysis [35, 36]. Similarly, we discovered *ZNF217* amplification in approximately 1.2% of patients, primarily those with prostate adenocarcinoma. Furthermore, the lack of DNA methylation of *ZNF217* predicted poor prognosis in breast cancer, independent of age and family history [37]. Consistent with these findings, our study found that *ZNF217* hypomethylation correlates with its overexpression in prostate cancer, potentially indicating poor prognosis and suggesting a causal link to the disease.

BNIP2, a member of the BCL2/adenovirus E1B 19 kd-interacting protein (BNIP) family, was first characterized for its role in protecting cells from virally-induced cell death. Previous studies widely recognized it as a tumor suppressor, since its pro-apoptotic activity in cancerous cells, resulting in favorable outcomes in patients with neuroblastoma or epithelial-derived cancer [38]. More recently, *BNIP2* has emerged as a highly conservative scaffold protein that binds RhoA protein, modulating cell kinetics and migration; loss of BNIP2 decreases RhoA activity and increased cell migratory behavior [39]. In our study, we observed that genetic deep deletions underlie the reduced *BNIP2* expression in tumor tissue. Yet our SMR analysis paints a seemingly opposite picture: the rs8040114 allele that increases *BNIP2* expression is causally associated with higher PrCa risk. We hypothesize a dual role for *BNIP2*: both as a tumor suppressor and as a gene influenced by germline variation, contributing to cancer predisposition. The SMR analysis might be capturing gene variants associated with *BNIP2* expression as the earliest somatic drivers of carcinogenesis, increasing susceptibility to PrCa in normal or pre-cancerous cells [40]. As cancer progresses, *BNIP2* may become silenced through epigenetic changes. Moreover, increasing evidence showed a multifaceted role of proapoptotic genes opposite to their conventional roles [41].

Our single-cell RNA sequencing analysis identified *BNIP2* as highly enriched in endothelial cells within the tumor microenvironment, with functional enrichment analyses linking it to pathways involved in endothelial cell migration, angiogenic regulation, and antigen processing and presentation. Correlation analyses further revealed that *BNIP2* expression exhibits moderate associations with CAFs and fibroblasts, while showing moderate-to-strong associations with various immune cell populations. These patterns suggest that *BNIP2* may primarily regulate intracellular functional programs within endothelial cells rather than directly mediating cell recruitment. Notably, *BNIP2*-expressing endothelial subsets displayed active interactions with epithelial cells, raising the possibility of their involvement in modulating epithelial cell behaviors. Collectively, these findings suggest a previously unrecognized role for *BNIP2* as a potential modulator of endothelial cell plasticity and point to its involvement in facilitating endothelial–immune and endothelial–epithelial crosstalk within the tumor milieu. However, the underlying mechanisms by which *BNIP2* governs endothelial cell behavior, and whether its functions vary across distinct tumor stages or microenvironmental contexts, remain to be elucidated. Future studies dissecting the stage-specific and context-dependent roles of *BNIP2* will be essential to fully understand its contribution to tumor progression and microenvironmental remodeling.

Lastly, our study identified *ZNF217* and *BNIP2* as potential therapeutic targets. We predicted doxorubicin (DOX), alsterpaullone, and camptothecin (CPT) as potential drugs targeting these genes. We verified their binding affinity through molecular docking simulations, which showed moderate to strong binding activity. Currently, these drugs are not routinely administered to patients with PrCa. Among the three drugs, DOX is

a classic chemotherapeutic drug for solid tumors and hematologic malignancies. We identified *ZNF217* and *BNIP2* as potential new targets for DOX, with PheWAS studies indicating no related cardiac side effects. This observation suggests new pathways for DOX's antitumor mechanisms. Alsterpaullone, a cyclin-dependent kinase (CDK) inhibitor, demonstrates suppressive effects on viral late genes and functions as an anti-tumor drug by inducing apoptosis in neurodegenerative and proliferative disorders [42]. CPT, a DNA topoisomerase inhibitor, exhibits robust antineoplastic activity against colorectal and ovarian cancers, among others. Recently, its prodrug—a nanoparticle-drug conjugate of CPT—has been developed for cancer therapy and used in clinical trials [43, 44]. However, drug repositioning of the above drugs for prostate cancer faces significant hurdles, most notably, the narrow therapeutic window imposed by their well-characterized off-target toxicities. Recent advances in nanoparticle-based delivery platforms, however, offer promising strategies to surmount these limitations. For example, a dual-aptamer silica nanoparticle assembly enabled selective uptake and apoptosis in both prostate-specific membrane antigen (PSMA)-positive and negative prostate cancer cells [45]. In a complementary approach, DOX-loaded mesoporous silica nanoparticles embedded within a thermos-responsive hydrogel demonstrated potent antitumor efficacy in a rat model of prostate cancer while substantially attenuating cardiotoxicity [46]. Similarly, encapsulating the PSA peptide-DOX prodrug in low temperature-sensitive liposomes effectively alleviated cardiac accumulation and improved pharmacokinetics under mild hyperthermia [47]. Collectively, these findings suggest that DOX, alsterpaullone, and CPT may exert potential epigenetic interventions on BNIP2 and ZNF217, potentially benefiting PrCa treatment, while the side effects might be overcome by harnessing nanoparticle platforms. Future studies should investigate the biodistribution and long-term safety to establish therapeutic window for repositioned chemotherapeutics.

The advantage of our study is that we used three distinct datasets to explore and validate SMR results using rather stringent criteria. The SMR method minimized reverse causality and confounding factors. Colocalization analysis enabled us to reduce bias due to linkage disequilibrium. Then, combining the mRNA sequencing dataset, we screened genes that putatively have a causal relationship with PrCa. Furthermore, epigenetic modulation and downstream effects of the key genes were investigated, supporting the important roles of the identified genes. However, it's important to acknowledge our limitations. First, the outcome dataset only included the European ancestry; further investigations of multi-ancestry are necessary. Then, the study mainly focused on cis-eQTLs in blood and their relationships with PrCa, potentially overlooking regulatory factors that contribute to the disease and tissue-specific effects. Further functional validation that investigates the mechanisms of key genes is required. Lastly, molecular docking simulation should be interpreted with caution, as off-target effects may exist. Though our PheWAS exploration demonstrated that the possibility is rather low.

This study explored potential causal relationships of gene expression with PrCa by integrating SMR analysis and differential expression analysis. Comprehensive analyses of prognostic significance, genetic alterations, immune cell infiltration, and pathway enrichment provided valuable insights into the roles of these genes in PrCa pathogenesis. Our drug prediction and molecular docking simulations highlighted potential therapeutic avenues for PrCa treatment. These findings deepen the pathogenesis of PrCa and provide potential therapeutic targets for pharmacological interventions.

Supplementary Information

The online version contains supplementary material available at https://doi.org/10.1186/s12575-025-00298-x.

Supplementary Material 1.

Supplementary Material 2.

Supplementary Material 3.

Supplementary Material 4.

Acknowledgements
The authors would like to thank all contributors of TCGA database and R packages used in this study for their valuable work. No artificial intelligence tools were used in the study.

Authors' Contributions
Study conception and design: Xuemeng Qiu, Zejia Sun, Wei Wang Data collection: Xuemeng Qiu, Xinyi Chai, Jiyue Wu. Analysis and interpretation of results: Xuemeng Qiu, Yifei Zhang, Jiyue Wu, Xihao Shen. Draft manuscript preparation: Xuemeng Qiu, Yifei Zhang, Zihao Gao. All authors reviewed the results and approved the final version of the manuscript.

Funding
The study was supported by grants from the Beijing Municipal Science and Technology Commission (No. Z221100007422029) and Clinical Research Incubation Project of Beijing Chao-yang Hospital, Capital Medical University (Project No: CYFH202203).

Data Availability
The study did not generate any original data. Codes used in the study are available upon reasonable request.

Declarations

Ethics Approval and Consent to Participate
Ethics approval is not required.

Competing Interests
The authors declare no competing interests.

Author details
[1]Department of Urology, Beijing Chao-Yang Hospital, Capital Medical University, 8 Gongrentiyuchang South Rd, Chaoyang District, Beijing 100020, China
[2]Institute of Urology, Capital Medical University, Beijing, China
[3]Beijing Children's Hospital, Capital Medical University, Beijing, China

Received: 28 March 2025 / Accepted: 29 July 2025
Published online: 16 October 2025

References

1. Prostate cancer. Nat Rev Dis Primers. 2021;7(1):8.
2. Culp MB, et al. Recent global patterns in prostate cancer incidence and mortality rates. Eur Urol. 2020;77(1):38–52.
3. Williams IS, et al. Modern paradigms for prostate cancer detection and management. Med J Aust. 2022;217(8):424–33.
4. Haffner MC, et al. Genomic and phenotypic heterogeneity in prostate cancer. Nat Rev Urol. 2021;18(2):79–92.
5. Sekula P, et al. Mendelian randomization as an approach to assess causality using observational data. J Am Soc Nephrol. 2016;27(11):3253–65.
6. Zhu Z, et al. Integration of summary data from GWAS and eQTL studies predicts complex trait gene targets. Nat Genet. 2016;48(5):481–7.
7. Wu Y, et al. Integrative analysis of omics summary data reveals putative mechanisms underlying complex traits. Nat Commun. 2018;9(1):918.
8. Nevedomskaya E, Haendler B. From omics to multi-omics approaches for in-depth analysis of the molecular mechanisms of prostate cancer. Int J Mol Sci. 2022. https://doi.org/10.3390/ijms23116281.
9. Sun W, et al. Associations between genetically predicted concentrations of plasma proteins and the risk of prostate cancer. BMC Cancer. 2024;24(1):905.
10. Desai TA, et al. Identifying proteomic risk factors for overall, aggressive, and early onset prostate cancer using Mendelian randomisation and tumour spatial transcriptomics. EBioMedicine. 2024;105:105168.
11. Wang QS, et al. Statistically and functionally fine-mapped blood eQTLs and pQTLs from 1,405 humans reveal distinct regulation patterns and disease relevance. Nat Genet. 2024;56(10):2054–67.
12. Qiu X, et al. Mendelian randomization reveals potential causal relationships between cellular senescence-related genes and multiple cancer risks. Commun Biol. 2024;7(1):1069.
13. Li Y, et al. Mitochondrial related genome-wide Mendelian randomization identifies putatively causal genes for multiple cancer types. EBioMedicine. 2023;88:104432.
14. Vosa U, et al. Large-scale cis- and trans-eQTL analyses identify thousands of genetic loci and polygenic scores that regulate blood gene expression. Nat Genet. 2021;53(9):1300–10.
15. Schumacher FR, et al. Association analyses of more than 140,000 men identify 63 new prostate cancer susceptibility loci. Nat Genet. 2018;50(7):928–36.
16. Chen S, et al. Single-cell analysis reveals transcriptomic remodellings in distinct cell types that contribute to human prostate cancer progression. Nat Cell Biol. 2021;23(1):87–98.
17. Tuong ZK, et al. Resolving the immune landscape of human prostate at a single-cell level in health and cancer. Cell Rep. 2021;37(12):110132.
18. Yoshihara K, et al. Inferring tumour purity and stromal and immune cell admixture from expression data. Nat Commun. 2013;4:2612.
19. Li T, et al. TIMER: A web server for comprehensive analysis of Tumor-Infiltrating immune cells. Cancer Res. 2017;77(21):e108–10.
20. Finotello F, et al. Molecular and pharmacological modulators of the tumor immune contexture revealed by deconvolution of RNA-seq data. Genome Med. 2019;11(1):34.
21. Becht E, et al. Estimating the population abundance of tissue-infiltrating immune and stromal cell populations using gene expression. Genome Biol. 2016;17(1):218.
22. Racle J, Gfeller D. EPIC: a tool to estimate the proportions of different cell types from bulk gene expression data. Methods Mol Biol. 2020;2120:233–48.
23. Szklarczyk D, et al. STITCH 5: augmenting protein-chemical interaction networks with tissue and affinity data. Nucleic Acids Res. 2016;44(D1):D380–4.
24. Kuleshov MV, et al. Enrichr: a comprehensive gene set enrichment analysis web server 2016 update. Nucleic Acids Res. 2016;44(W1):W90–7.
25. Yoo M, et al. Dsigdb: drug signatures database for gene set analysis. Bioinformatics. 2015;31(18):3069–71.
26. Shu F, et al. M6A modification promotes EMT and metastasis of castration-resistant prostate cancer by upregulating NFIB. Cancer Res. 2024;84(12):1947–62.
27. Ma X, et al. SLC39A1 overexpression is associated with immune infiltration in hepatocellular carcinoma and promotes its malignant progression. J Hepatocell Carcinoma. 2022;9:83–98.
28. Wang P, et al. *SLC39A1* contribute to malignant progression and have clinical prognostic impact in gliomas. Cancer Cell Int. 2020;20(1):573.
29. Li Y, et al. ZNF217: the cerberus who fails to guard the gateway to lethal malignancy. Am J Cancer Res. 2021;11(7):3378–405.
30. Briest F, et al. Frequent ZNF217 mutations lead to transcriptional deregulation of interferon signal transduction via altered chromatin accessibility in B cell lymphoma. Leukemia. 2023;37(11):2237–49.
31. Xu LM, et al. Microrna-135 inhibits initiation of epithelial-mesenchymal transition in breast cancer by targeting ZNF217 and promoting m6A modification of NANOG. Oncogene. 2022;41(12):1742–51.
32. Fahme P, et al. The Intricate Interplay between the ZNF217 Oncogene and Epigenetic Processes Shapes Tumor Progression. Cancers (Basel). 2022;14(24):6043
33. Szczyrba J, et al. Identification of ZNF217, hnRNP-K, VEGF-A and IPO7 as targets for MicroRNAs that are downregulated in prostate carcinoma. Int J Cancer. 2013;132(4):775–84.
34. Jiang X, et al. GATA3-driven expression of miR-503 inhibits prostate cancer progression by repressing ZNF217 expression. Cell Signal. 2016;28(9):1216–24.
35. Krig SR, et al. *ZNF217*, a candidate breast cancer oncogene amplified at 20q13, regulates expression of the *ErbB3* receptor tyrosine kinase in breast cancer cells. Oncogene. 2010;29(40):5500–10.
36. Kuo KT, et al. DNA copy numbers profiles in affinity-purified ovarian clear cell carcinoma. Clin Cancer Res. 2010;16(7):1997–2008.
37. Widschwendter M, et al. Epigenotyping in peripheral blood cell DNA and breast cancer risk: a proof of principle study. PLoS One. 2008;3(7):e2656.
38. Tatsumi Y, et al. BMCC1, which is an interacting partner of BCL2, attenuates AKT activity, accompanied by apoptosis. Cell Death Dis. 2015;6(1):e1607.
39. Pan M, et al. BNIP-2 retards breast cancer cell migration by coupling microtubule-mediated GEF-H1 and RhoA activation. Sci Adv. 2020;6(31):eaaz1534.
40. Emami NC, et al. Association of imputed prostate cancer transcriptome with disease risk reveals novel mechanisms. Nat Commun. 2019;10(1):3107.
41. Ghorbani N, et al. How does caspases regulation play role in cell decisions? Apoptosis and beyond. Mol Cell Biochem. 2024;479(7):1599–613.
42. Watanabe T, et al. Antitumor activity of cyclin-dependent kinase inhibitor Alsterpaullone in Epstein-Barr virus-associated lymphoproliferative disorders. Cancer Sci. 2020;111(1):279–87.
43. Zhang L, et al. Glutathione-responsive nanoparticles of camptothecin prodrug for cancer therapy. Adv Sci (Weinh). 2023;10(3): e2205246.
44. Schmidt KT, et al. A Single-arm phase II study combining NLG207, a nanoparticle camptothecin, with enzalutamide in advanced metastatic Castration-resistant prostate cancer Post-Enzalutamide. Oncologist. 2022;27(9):718–e694.
45. Min K, et al. Dual-aptamer-based delivery vehicle of doxorubicin to both PSMA (+) and PSMA (-) prostate cancers. Biomaterials. 2011;32(8):2124–32.
46. Silveira CP, et al. Doxorubicin-functionalized silica nanoparticles incorporated into a thermoreversible hydrogel and intraperitoneally administered result in high prostate antitumor activity and reduced cardiotoxicity of doxorubicin. ACS Biomater Sci Eng. 2016;2(7):1190–9.
47. Pereira S, et al. Encapsulation of doxorubicin prodrug in heat-triggered liposomes overcomes off-target activation for advanced prostate cancer therapy. Acta Biomater. 2022;140:530–46.

Publisher's Note